Microfluidic Assays to Enhance Biodetection and Diabetes Research

by

Kai Duan

A thesis submitted in partial fulfillment

of the requirements for the degree of

Master of Science in Engineering

(Bioengineering)

in the University of Michigan-Dearborn

2018

Master's Thesis Committee:

Assistant Professor Joe Fujiou Lo, Chair

Associate Professor Gargi Ghosh

Associate Professor Yasha Yi

ACKNOWLEDGEMENTS

I would like to thank for the great support of Prof. Joe Lo-University of Michigan-Dearborn. Thank for the help of Prof. Gargi Ghosh-University of Michigan-Dearborn. Thank Zhengtuo zhao for training me in bioengineering lab. Thank for other lab members for their time and assistance: Rui Liu, Di Hu, Mengyang Zhou, Luwei Zou, Jessica Hallgath. I would also like to thank for the supports from NIH 1R03EB023459 grant and the University of Michigan at Dearborn Office of Research.

TABLE OF CONTENTS

LIST OF FIGURES

ABSTRACT

Expansion of biomarker detections with nuanced monitoring of disease states can deliver more effective, personalized medicine. Leveraging novel biomarkers in clinical settings requires higher sensitivity, shorter assay times, and increased specificity in protein detection. Standard ELISA involves multi-step preparations that extends the length and complexity of its protocol. Newer techniques using nanoplasmonics, fluorescence resonance energy transfer, single molecule detections, among others require specialized equipment and techniques. Here I report a novel method using immuno-functionalized, porous poly (ethylene) glycol diacrylate (PEGDA) hydrogel microspheres to enable rapid, high sensitivity antigen detection in arrayed microfluidics. I applied these microfluidic techniques to wound healing and diabetes motivated applications that illustrate their future potentials.

In wound healing, Vascular endothelial growth factor (VEGF) promotes wound revascularization by stimulating angiogenesis, in addition to stimulatory effects on other wound cells. In our arrayed microfluidics, the technique incorporates antibody encapsulation, trapping, and flow perfusion on a single device to allow an integrated assay. The result showed that the convergence of tunable porous hydrogel with efficient microfluidics improved the sensitivity of the assay. The detection limit of this microfluidic porous microgel based assay

was 0.9 pg/mL, with only 1+ hour of assay time, demonstrating a novel assay that exceed conventional technologies in terms of sensitivity and speed.

In the multifaceted disease of diabetes, sensitive, single volume detections of multiple antibodies can provide immunoprofiling and early screening of at-risk patients. To advance the state-of-the-art suspension assays for diabetes antibodies, porous hydrogel droplets were multiplexed in microfluidic serpentine arrays to enhance the detection of antibodies against insulin, glutamic acid decarboxylase (GAD), and insulinoma-associated protein 2 (IA-2). Optimization of assay protocol resulted in a shortened assay time of 2 h, with better than 20 pg mL detection limits across all three antibodies. Specificity and cross-reactivity tests showed negligible background, nonspecific antibody–antigen, and nonspecific antibody–antibody bindings. Multiplexed detections were able to measure within 15% of target concentrations at both low and high ranges. The technique enabled quantifications of as little as 8000 molecules in each 500 μm droplet using a single volume, multiplexed assay format, a breakthrough necessary for the adoption of diabetes panels for clinical screening and monitoring in the future.

Also, the PEGDA hydrogel sensors is being applied in our latest diabetes project: Hypoxia-FFA synergy in beta cell impairment via multimodal microfluidics. To achieve the beta cell culture and precise detection of insulin, a porous PEGDA hydrogel biosensor thin film was developed for coating on microfluidic devices. This new spatial sensor is able to enhance the detection of secreted insulin transport, while mapping their release in beta cells cultured atop a gradient of oxygen concentrations. The optimization of this multimodal device resulted in a

200 um thickness sensor, shorten assay time of 2 hours, better than 50 pg/mL detection limits, and capable of sustaining better than 90% viability of beta cells.

Chapter 1: Device Fabrication

BACKGROUND

Microfluidic covers a wide range of engineering, biotechnology and nanoscale technologies, and leverage many phenomena such as small volumes, small size, low energy consumption and effects of the microdomain. To address the advance of microfluidic in bioengineering, the microfluidic design has been centrally applied in micro and nano structure to manipulate minute volumes of fluids. The history of microfluidic started ca. 1950s, e.g. their utility in tiny tubes that transport ink for printing technology. Later in 1960s technology like photolithography were developed, allowing to integrate thousands of transistors on semiconductor wafers. With a continued development, in 1990s researchers investigated the applications of Micro Electro Mechanical Systems (MEMS) in biology field in order to control of liquids in microchannels. Then in early 2000s, there was a great expansion of microfluidic technology based on molding microchannels in polymers like PDMS. Due to the reduction of costs and production time of making microfluidic devices, a large number of laboratories were able to conduct microfluidic research using micro-pump, mixer and other devices Droplet based microfluidic is a rapidly growing field of biomedical research, which can be applied in diseases diagnostics, protein crystallization and living cells culture. One major advantage of

droplet based microfluidic is that the droplet volumes and individual droplet contents can be precisely controlled Recently, precise generation and repeatability of droplet operations and enhanced reaction rates have made droplet based microfluidic system a proper platform for biomedical researches and applications.

Molecule gradients play an important role in physiology and pathological phenomena, for example, the gradients can be applied in immune response, wound healing, development and cancer metastasis. In biomedical applications, researchers used a range of engineering tools to develop the cellular microenvironment to characterize cellular responses to gradients. Microfluidic based gradients have unique advantages in precise manipulation of multiple parameters spatially, capable of generating both 2D and 3D gradient for cellular microenvironment. Microfluidic gradients opens a new way to control different cellular environment at the micro-scale.

MICROFLUIDIC DEVICE FABRICATION METHOD

Microgel droplet generator

The most common way for microfluidic device fabrication is photolithography. To make our microgel droplet generator device, we used PDMS soft photolithography method. As soft photolithography can process a wild range of elastomeric materials, PDMS has been the most wildly used material, because its useful features like low costs, biocompatibility, low toxicity, chemical inert and mechanical flexibility.

The basic processes of photolithography include wafer cleaning and preparation, photoresist spin coating, baking, UV exposure and developing. The processes of PDMS soft photolithography include PDMS mixing, pouring, baking, hardening, peeling and bonding **(Figure 1)**.

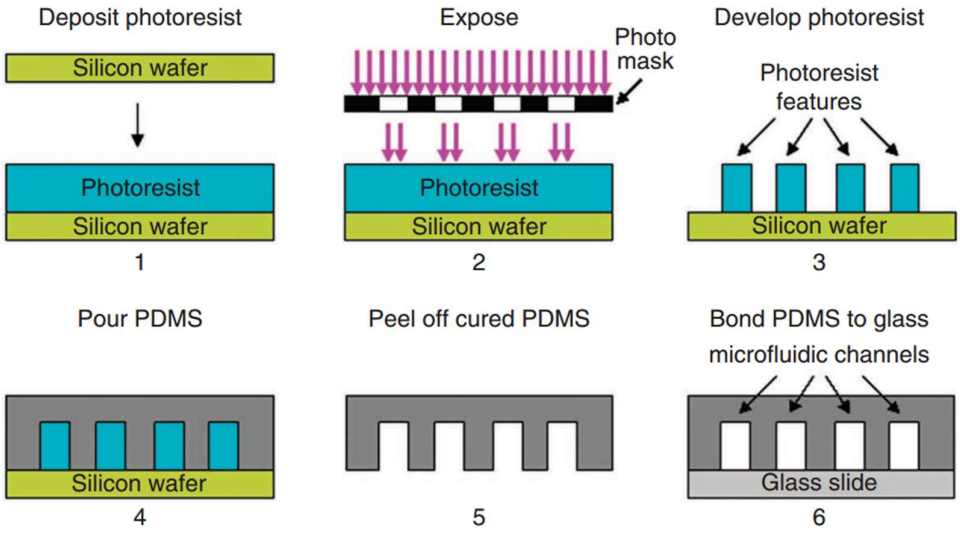

Figure 1. Photolithography and PDMS soft lithography steps

For fabricating the microgel generator device in this study, the microgel generator microfluidic designed by AutoCAD, and then print on a transparent photo mask **(Figure 2)**.

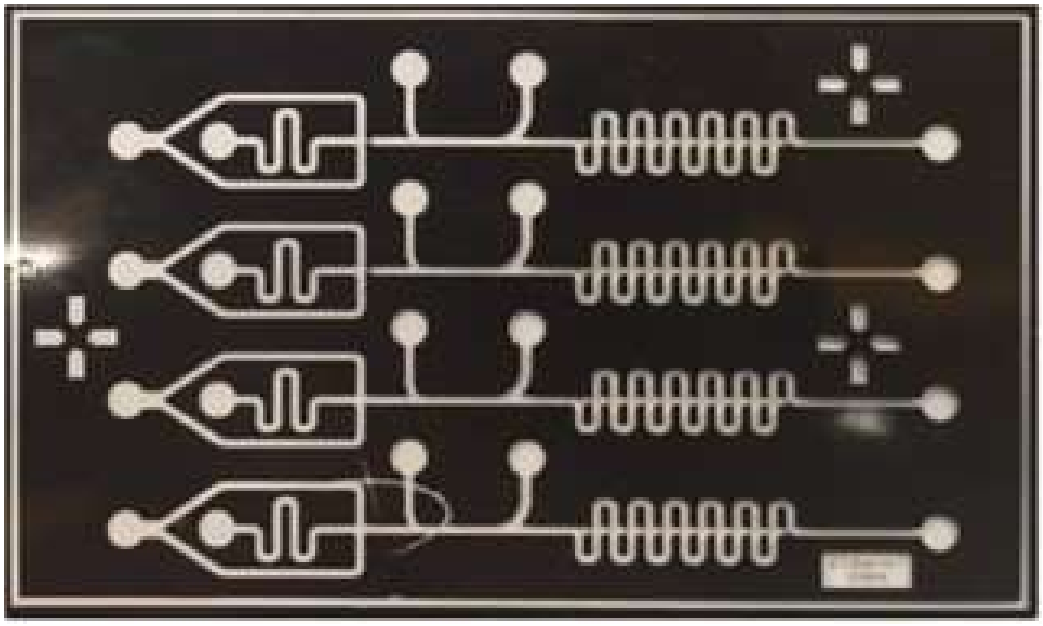

Figure 2. AutoCAD designed photo mask for microgel generator device.

To do the photolithography, SU-8 (from Microchem, Inc) was spun on a 4'' silicon wafer to yield a 500 μm thickness, then baked on a 65℃ohotplate for 10 minutes, after that, baked at 90℃0hotplate for 120 minutes. Next, the SU-8 coating was covered the with the designed photomask, and UV light was exposed through the mask at 600 mJ/cm 2. Then, the wafer was submerged in the solvent developer to remove the excess photoresist for 30 minutes, leaving just the channel pattern on the wafer.

After SU-8 photolithography, we mixed the PDMS pre-polymer at 1:10 curing agent to monomer ratio, which was then poured onto the master wafer and cured at 95℃ for 120 minutes. The curing resulted in a PDMS layer with channels, which can then be bonded to a glass slides using oxygen plasma bonding. After the whole processes, a cross-junction microgel droplet generator and a serpentine trapper array were fabricated. The channel geometry was

defined as 550×500 μm (W×D) channels. The width of the orifice at cross-junction is 150 μm. In addition, the devices were also baked on 200 °C for 1 h to help the recovery of hydrophobicity before using.

Gas gradient generator

To make the gas gradient generator device, a rectangle gradient was designed with 20 lines in each side to mimic rectangular geometry, we also use PDMS soft photolithography. For the fabrication of gas gradient microfluidic device, The SU-8 coating is 200 μm thickness, premixed PDMS was spun coating at 900 rpm on the wafer for twice, then cured and bonded to the glass slides, to get the gas gradient diffusion channel, after that, bonded another PDMS slice on the top with cell culture chamber. After the fabrication, the device was flow in oxygen and nitrogen from oxygen inlet and nitrogen inlet to form the gas gradient.

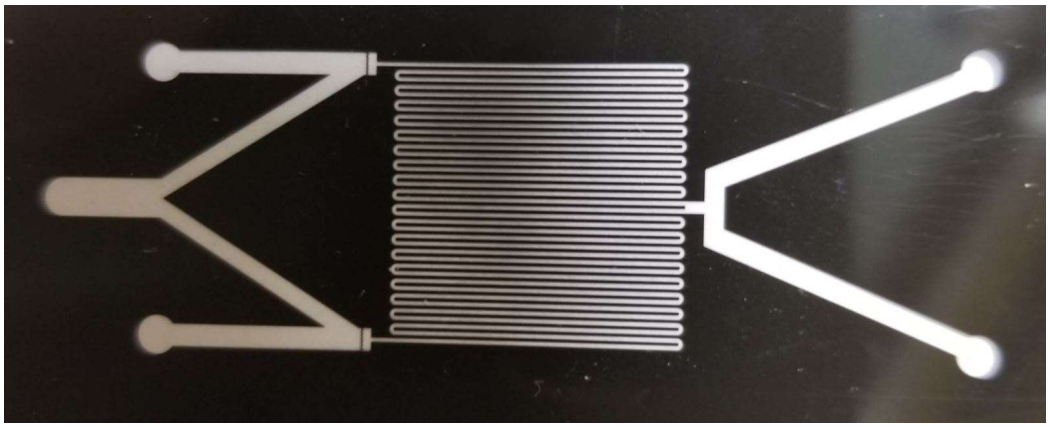

Figure 3. AutoCAD designed photo mask for gas gradient device.

Chapter 2: Development Work of a Microfluidic Porous Microgel Detection Platform

The whole research was finished by Zhengtuo Zhao, Mohammad Ali Al-Ameen and me, refer to the publication 'On-chip porous microgel generation for microfluidic enhanced VEGF detection' in Biosensors and Bioelectronics journal

INTRODUCTION

Advances in biomedical diagnostics require sensitive yet robust methods for rapid measurement of proteins and biomolecules like vascular endothelial growth factor (VEGF) as disease biomarkers. This study as a background research for the verification of our microfluidic porous droplet method in protein detection, especially focusing on the VEGF detection in microfluidics with VEGF antibody immobilized porous microgel, and fluorescence by reporter antibody labeled.

The binding of VEGF to its receptors initiates signaling cascades which regulate the endothelial cellular processes including migration, proliferation, and formation of new blood vessels from pre-existing vessels [72; 80; 87]. In chronic wounds, VEGF promotes wound

healing by stimulating angiogenesis. In addition, the mitogenic as well as chemotactic effects of VEGF facilitate in the closure of the wound with compromised vascularity [68]. Thus, quantifying and profiling VEGF over time have implications as biomarker for different clinical disorders. Although enzyme-linked immunosorbent assay (ELISA) remains the corner stone for protein quantification, the technique has been labor intensive and out-paced by the requirements of rapid clinical detections.

Sandwich ELISA has stringent requirements for assay preparations and procedures, making the technique labor intensive and error prone. To address shortcomings of ELISA, microarray-based technologies have quickly emerged as an excellent alternative for achieving high-throughput and high content biomarker detection due to advantages such as fast analysis, low sample consumption, effective cost, and portability [78; 81; 84; 84; 91; 93]. These include novel substrates, probe designs, and new sensor material to improve VEGF detections [75; 92; 98; 104]. However, fixed design, long incubation times, and low flexibility still limit their applications in clinical settings. In recent years, conventional paradigm of planar microarrays has evolved into novel suspension arrays [67; 73; 79; 86; 96; 106], which offer the advantages of higher flexibility by simply changing/adding probe particles, enhanced reaction kinetics due to radial diffusion, shorter incubation and assay times, less sample consumption, and lower cost. Suspension arrays involving polystyrene beads doped with combinations of dyes for optical coding have been developed by Luminex [70]. Moreover, suspension array technologies with barcodes, Au/Ag nanobarcodes, silica nanotubes, dot-coded polymer particles, and

Ilumina's VeraCode have been developed to further improve their multiplexed readouts [67; 70; 74; 86; 106]. In addition, our previous work [67] created tunable, porous hydrogel particles in an effort to improve diffusion kinetics while keeping the benefits of hydrogel suspension assays. We were able to decrease assay times while reducing non-specific protein adsorption and retaining hydration to improve antibody activity, due to the bio-inertness of the water-laden hydrogels. The resulting assay protocol, though more time-efficient, was not tailored to the micro-sized porous substrates, where the mass transport was limited by bulk reagent agitation and mixing. Additionally, manual manipulation of the micro-sized substrates is difficult and time taxing. The next breakthrough of our porous microgel assay, then, requires an efficient, high fidelity, and precisely arrayed microfluidics.

Naturally, microfluidics is the next step to evolve our porous microgel assays with precisely generated and manipulated microgel droplets. Its innovation goes beyond integration and leverages enhanced molecular transport towards faster and more precise reagent handling and detection. In this work, a microfluidic droplet generator was integrated with a serpentine trapper array, enabling precise reagent handling to be applied to tunable microgel droplets **(Figure 4)**. As a result, the all-in-one device achieved rapid and sensitive VEGF detection and verified the our microfluidic porous microgel method as a competitive protein detection panel.

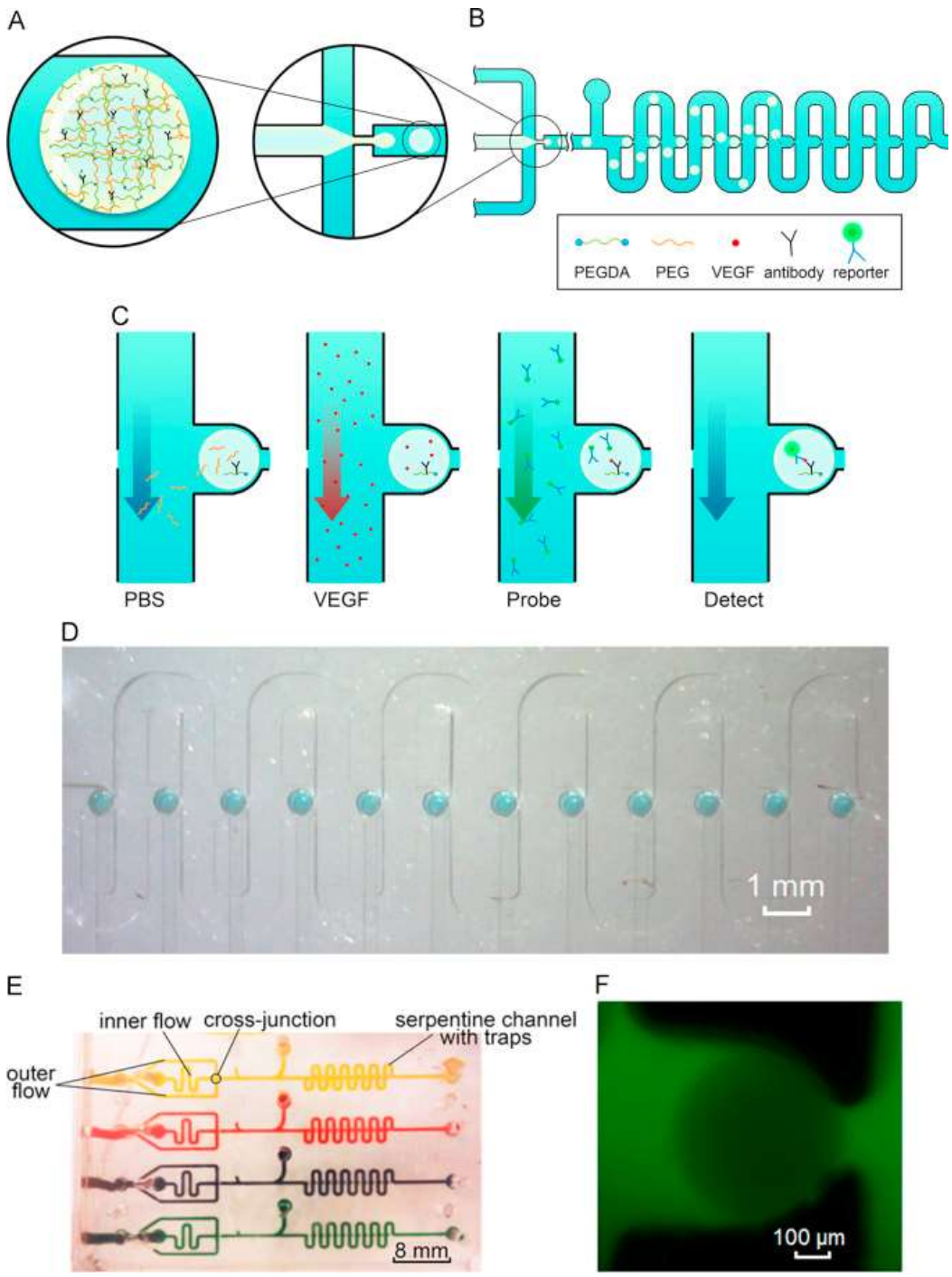

Figure 4. Schematic of the detection system.

(A) The microfluidic droplet generator allowed on-chip generation and tuning of porous

microgel droplets, with well-controlled spherical shapes and volumes. (B) Droplet generator was integrated with a serpentine trapper array to precisely position the generated microgel droplets. (C) Moreover, it allowed trapped droplets to be shielded from reagent flow in the serpentine channel, enabling predictable microfluidic enhanced mass transport for assay protocols. (D) This resulted in a row of trapped droplets for protein assays (colored in blue with food dye). (E) In the prototype, 4 rows of 12 droplets each, totaling 48 traps, were achieved to demonstrate the array scalability (actual device with yellow, red, purple and green food dye in channels). (F) Each trap site contained a single porous microgel droplet with predictable assay kinetics, as shown by 250 kDa FITC dye penetration.

MATERIALS AND METHOD

Materials

Poly (ethylene glycol) diacrylate (PEGDA) (Min.~6000, referred as PEG6000DA), poly (ethylene glycol) (PEG) (Min.~20,000), fluorescein isothiocyanate—dextran (FITC-Dextran 250 KDa), mineral oil, phosphate buffer saline (PBS), and IgG from human serum were procured from Sigma-Aldrich (St. Louis, MO). Human vascular endothelial growth factor (VEGF), anti-hVEGF antibody, and Alexa Fluor 488 conjugated anti-hVEGF antibody were purchased from R&D systems (Minneapolis, MN). Fetal bovine serum (FBS) was procured from Gibco. Polydimethylsiloxane (PDMS) was obtained from Ellsworth adhesives and SU8 2100 was purchased from MicroChem.

Methods

To immobilize the antigens within the microgel, the antigens were incubated with 1.25 mg of ACRL-PEG-SCM-5000 in PBS at room temperature for 3 h prior to use and discarded afterward. The prepolymer solution consisting of 100 μL of 8% (w/v) of PEG6000DA, 2% (w/v) photoinitiator, 10% (w/v) PEG 20K, and acrylated antigen was then loaded in the microfluidics for droplet generation.

The prepolymer solution was introduced at 1 μL min−1, and mineral oil was introduced at 15 μL min−1 to generate the droplets at the microfluidic cross-junction. When one of the generated droplets was flown in to the serpentine pockets, its trapping blocked the cross-serpentine flow and redirected the next droplet toward the following pocket sequentially. After trapping, droplets were exposed to ultraviolet light for crosslinking for 5 min (UVP CL-1000 UV Oven, 365 nm). Then, BSA buffer was flown in at 30 μL min−1 to continuously wash the droplet for 30 min to prevent PDMS protein absorption. Lastly, PBS was flown in at 30 μL min−1 to continuously wash the droplets for 4 h to remove the unreacted reagents and PEG porogens, thus creating the porous microgel.

RESULTS AND DISCUSSION

All experiments were carried out with VEGF antibody immobilized porous microgel droplets generated with 10% PEG 20KDa porogen. These particles were incubated with

varying concentration of VEGF flow (30 µl/min) in microchannel for 30 minutes, washed, and then incubated with Alexa Fluor 488 conjugated anti-VEGF antibody flow (30 µl/min) for 45 min. After washing the microgel droplets to remove the unbounded reporter antibody, the fluorescence intensities from the microgel droplets were accessed using Zeiss Axio Observer microscope. Their fluorescence signal was quantified as described in the methods section.

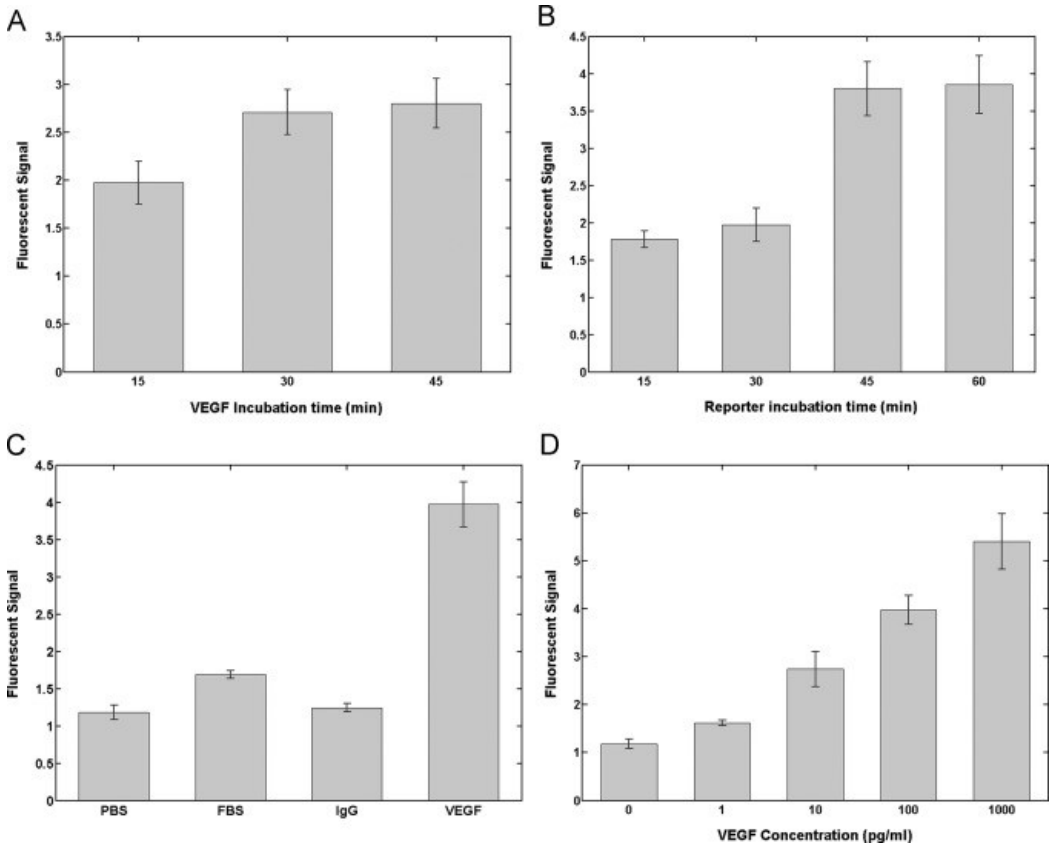

Figure 5. VEGF assay via microfluidic porous microgels.

Incubation times were optimized before characterizing the VEGF detection. (A) VEGF protein incubation times above 30 min reaches a stable signal readout. (B) Reporter incubation times

above 45 min reaches a stable signal readout. Thus, 30 min VEGF and 45 min reporter incubation times were used to for subsequent VEGF detections. (C) Specificity of the VEGF assay was demonstrated by incubating the microgel droplets with FBS, 100 g/mL IgG, and 100 pg/mL VEGF. (D) VEGF detection in microfluidic enhanced porous microgels yielded a detection curve from 1 to 1000 pg/mL. Using this trend, a detection limit of 0.9 pg/mL was calculated (at 3 times the SD above 0 pg/mL). Error bars denote standard deviations.

Optimization of VEGF and anti-VEGF incubation time

To optimize the reaction time, microgel droplets were incubated with Alexa Fluor 488 conjugated anti-VEGF antibody for 30 min and 100 pg/mL VEGF for times ranging from 15 to 45 min. Subsequently, microgels were incubated with 100 pg/mL VEGF for 30 min and Alexa Fluor 488 conjugated anti-VEGF antibody for times ranging from 15 to 60 min. **Figure 5A** illustrates the time dependent fluorescent signal, indicating interaction between VEGF and capture antibody. As expected, protein-antibody interaction increased with increase in reaction time from 15 to 45 min. However, the fluorescent signal obtained following incubation of the droplets with VEGF for 45 minutes was not significantly different from that obtained upon 30 min incubation, indicating that the fluorescent signal saturated by 30 min. As significantly higher fluorescent intensity was observed following 30 min VEGF incubation, all subsequent experiments were carried out with a VEGF incubation time of 30 min. **Figure 5B** illustrates the time dependent fluorescent signal indicating interaction between VEGF and anti-VEGF antibody. As expected, protein-antibody interaction increased with increase in reaction time from 15 to 60 min. However, the fluorescent signal obtained following incubation of the droplets with VEGF for 60 min was not significantly different from 45 minutes incubation

indicating that the fluorescent signal saturated by 45 min. As significantly higher fluorescent intensity was observed following 45 min anti-VEGF antibody incubation, all subsequent VEGF experiments were carried out with an anti-VEGF antibody incubation time of 45 min.

Determining specificity of the microgel assay

One of the major difficulties in protein assay is the rise of fluorescent signal, either due to nonspecific adsorption within microgel droplets or due to nonspecific interaction with immobilized antibody. To further investigate whether other components of serum can affect fluorescent signal, VEGF antibody immobilized microgel droplets were incubated with 100 pg/mL IgG in PBS, FBS, and 100 pg/mL VEGF for 1 h, **Figure 5C**. In particular, the comparison of VEGF detection with non-specific background proteins in FBS provides a proof-of-concept demonstration for clinical applications involving blood and serum. Furthermore, future work can integrate on-board microfluidics for sample preparation to yield a purified sample for better detections. A high signal was obtained for 100 pg/mL VEGF (3.85), low signal for FBS (1.5) and almost no significant signal obtained upon incubation with IgG (1.25). This indicated that proteins other than VEGF have minimum contribution towards the fluorescent signal. Moreover, this established that the immobilization of antibody within the microgel droplet is sufficient for specificity, without additional protein blocking, which reduces the complexity of the assay.

Determining detection limit of the microgel assay

After confirming the fluorescent signal observed was primarily due to interaction between VEGF and antibody, the detection limit of the assay was characterized by exposing the microgel droplets to 0–1000 pg/mL VEGF solutions for 30 min. As demonstrated in **Figure 5D**, fluorescent signal increased with increase in VEGF concentration. The overall signal increased from 1.4 to 6.0 upon varying VEGF concentration from 1 pg/mL to 1000 pg/mL. The minimum concentration of VEGF detectable by this assay was considered to be the concentration at which the signal deviated from the average signal obtained in absence of VEGF by three times the standard deviation. Using this definition, the detection limit of this assay was found to be 0.9 pg/mL, which can be attributed to the precise control of microfluidic mass transport, leading to smaller errors and thus a lowered limit of detection. This improved sensitivity and shortened the assay time excels over the conventional ELISA and Luminex assays, as well as our previous work in porous microgels **(Figure 6)**.

Comparison with standard VEGF ELISA

ESLIA assays have high credibility due to their demonstrated coefficient of variation (CV). Human VEGF kit from R&D Systems, for example, has an inter-assay CV of 5–8% and intra-assay CV 3–6%. We examined the 100 pg/mL assays with n=6 separate runs, and arrived with inter-assay CV of 13.1%, while the intra-assay CV is 8.75%. These results show that our assay is approaching the confidence level of the well-established ELISA assay.

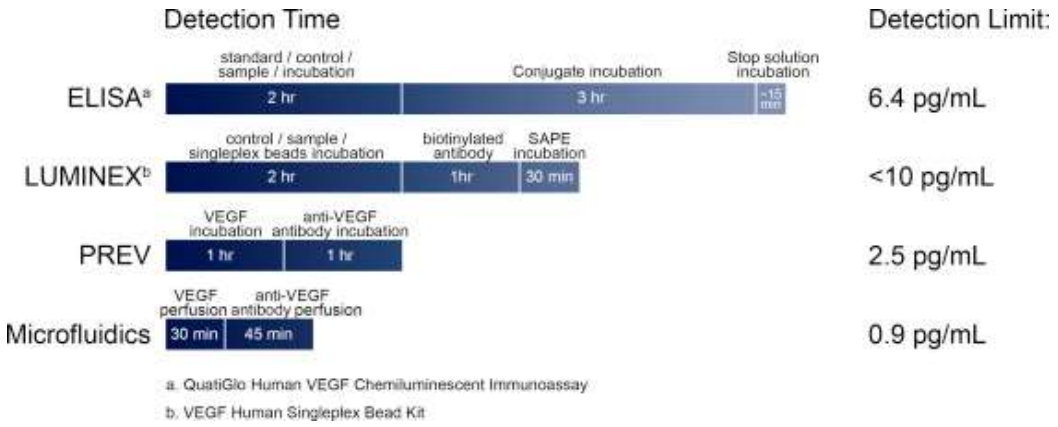

Figure 6. Comparison with ELISA, Luminex assays and previous study.

Microfluidic porous microgel VEGF assay provided the lowest limit of detection at 0.9 pg/mL and shortest assay time of 1+ hours, compared to aforementioned techniques.

CONCLUSION

In this study, we have leveraged microfluidic scaling with enhanced molecular transport of porous hydrogels, precisely generated microgel droplets within an integrated serpentine trapper array. We optimized the incubation times down to 1+ hours and demonstrated a breakthrough in assay sensitivity of 0.9 pg/mL without the need for protein blocking. In conclusion, our results shows that with our microfluidic porous microgel platform the mass transport are enhanced. Compare with the traditional protein detection method, a rapid and sensitive detection could be achieved, in this way lead to a solution for next generation of quantitative

protein assay via the synergistic combination of microfluidics and porous microgel.

Chapter 3: Microfluidic Porous Microgel Platform Enhanced Diabetes Autoantibodies Detection

This research project is mainly focusing on the diagnostics of Type I diabetes, refers to my publication 'Optimizing Multiplexed Detections of Diabetes Antibodies via Quantitative Microfluidic Droplet Array' in Small journal.

INRODUCTION

We have created porous polyethylene glycol (PEG) hydrogel—"smart microgels"—to enhance the diffusion of biomolecules within the droplets, achieved rapid detection of proteins using our microfluidic porous microgel platform.[48-51] Take the advances of our microfluidic porous microgel platform in disease diagnostics, we further improved our method achieving multi-detection to enable the detection of diabetes related autoantibodies.

It's of great interest that how rising levels of diabetes autoantibodies are related to Type I diabetes (T1D) disease pathogenesis. Detection of diabetes autoantibodies enables clinical diagnosis of T1D,[1-10] to provide predictive and screening values, sensitive detections is strongly needed.[10-13] Autoantibodies against insulin, glutamic acid decarboxylase (GAD),

and insulinoma associated protein-2 (IA-2) are well established in T1D panels, and thus are targeted in multiplexed detections.[14, 15] In clinical, around 54% to 75% T1D are with the presence of IA-2 antibodies.[16] Additionally, 66% of newly diagnosed patients test positive for insulin autoantibody.[17] Testing for a panel of aforementioned antibodies using sensitive detections can identify better than 85% of disease presentation or future T1D development with 98% specificity.[18] Moreover, more than 80% of diabetes in young children are accounts for T1D.[19] Unsettlingly, development of T1D in children is especially acute, with afflicted children showing severe symptoms, very high blood glucose, marked glycosuria, and ketonuria.[20, 21] Incidentally, the rise of autoantibodies manifests very early, with transients observable before 1 year of age **(Figure 7A)**, providing a strong marker for clinical diagnosis and screening for T1D.[22] For these young patients, earlier diagnosis or even predictive screening may mean critical disease management before manifestation of life-threatening symptoms. Current understanding of these diabetes autoantibodies points to a potential neoantigen immunogenicity,[23-26] where stress-modified protein synthesis leads to new epitopes on autoantigens that enhance their bindings to antibodies[27-31] or elicit cell-mediated immune responses.[32-36] Thus, sensitive detection of insulin, GAD, and IA-2 autoantibodies can serve as a powerful diabetes panel to monitor T1D disease progression, as well as investigate the mechanisms of beta cell autoimmune dysfunctions.

The standard detection methods for diabetes autoantibodies include radioimmunoassays (RIAs) and enzyme-link immunosorbent assays (ELISAs). Serum RIA and ELISA protocols

uses semi-quantitative titrations with varying sensitivities, which may not be useful for early or new-onset diabetics.[37] In practice, RIA is time consuming and labor intensive, while ELISA requires multiple sample preparations to provide multiplexed detection of autoantibodies.[1, 5] Moreover, there is a need for a uniform method of quantitative detections of all three antibodies in a single volume. For example, serum autoantibody levels can be measured in dilution titers (e.g., Juvenile Diabetes Foundation units), RIA percentage, or in enzymatic U mL^{-1}, with various cutoff definitions for positive detections.[1, 5, 15, 38] As a comparison, normal serum levels of all three autoantibodies are nominally regarded as 0.02×10^{-9} M (e.g., 2.4 ng/mL for insulin IgG) or lower by the World Health Organization and Mayo Clinic Interpretive Handbook.[39] Nevertheless, the cutoffs established by the various methods represent the diagnostic levels of T1D, whereas early screening would call for greater sensitivity to detect earlier transients.

Toward improving diabetes autoantibody detections, advances have been made via multiplexed microarrays[15] and electrochemiluminescence (ECL) assays.[14, 40, 41] Diabetes microarrays enabled single serum preparation for a multiplexed antibody detection panel, while ECL assays pushed the quantitative autoantibody detections below 10−11 mole/L (ng/mL) range, respectively. However, these separate improvements to autoantibody detections have not yet offered a combined sensitivity and multiplexing in a single volume assay.

We addressed these needs for the diabetes detection panel by creating multidetection based on our microfluidic porous microgel, we have demonstrated that the porosity generated by 20

kDa PEG optimized the diffusion of 250 kDa fluorescein isothiocyanate (FITC)-dextran into the hydrogel. This is larger than the 65 kDa antibodies used in this multiplexed assay, ensuring analyte access through the droplet volume. To achieve the multiplexing, different prepolymers containing different acrylated antigens were loaded in the microfluidic tubing, and introduced into microfluidic channel to generate the droplet, and then the multi-generation of droplets was achieved by flow switching and droplet redirection. The multiplexed diabetes detection platform was optimized with recombinant proteins and antibodies to push the performance envelop of detections, toward serum measurements in the future. The result is a quantitative, faster, and single sample multiplexed detection panel for insulin, GAD, and IA-2 antibodies. Finally, the platform can be easily adapted for future antibodies such as zinc transporter 8.[52-54] Potential clinical applications of this detection panel may enable detailed immune profiling in T1D, and pave the way for a robust tool for early screening.

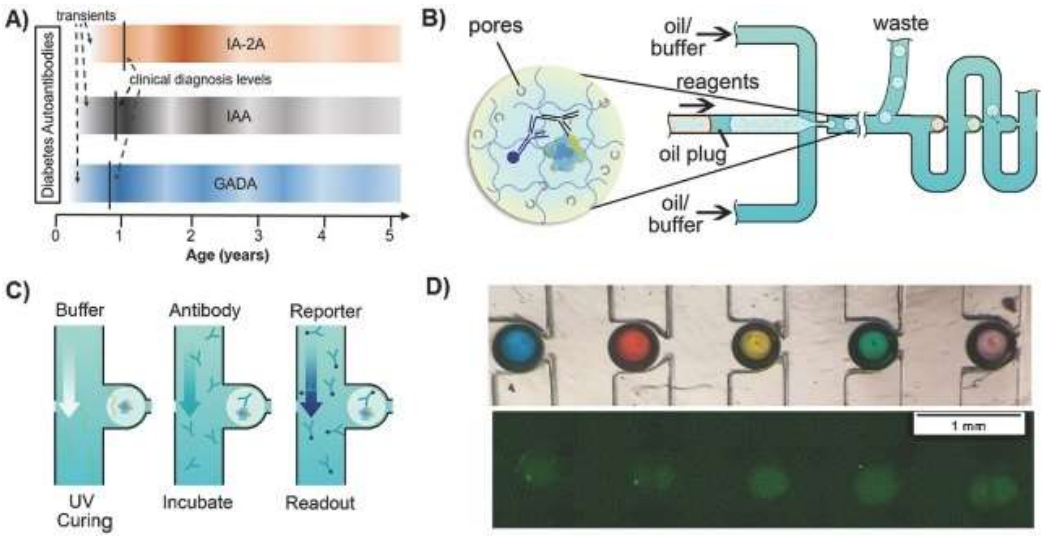

Figure 7. Quantitative microfluidic droplet array for diabetes detection panel.

A) The rise and change of diabetes autoantibodies vary in individuals, can be observed as early as 1 year of age, demonstrating the need for sensitive detection of multiple autoantibodies. B) We engineered a microfluidic array that generated individual porous droplets with detection chemistries optimized for the insulin, GAD, and IA-2 antibody detections. These porous microgels were then directed to designated traps within the serpentine channels. This spatial multiplexing was achieved by flow switching of unwanted droplets to a waste channel, redirecting droplets back toward the traps when the correct detection chemistry is generated. C) The serpentine microchannels allowed trapped droplets to be perfused by assay reagents. Buffer perfusion after UV curing allowed the porogen molecules (yellow stripes) to be washed away, creating a porous hydrogel droplet. Target antibodies (blue) and reporter antibodies (green) were then subsequently introduced into the microchannels, completing the immunoassay protocol. D) The result of spatial multiplexing was an array of droplets targeting individual diabetes antibodies, illustrated on top by the generation of multicolored droplets using food dyes. In the actual assay on bottom, only a single reporter wavelength was required, providing fluorescence intensities that varied at each spatial position per its respective antibody detection.

MATERIALS AND METHODS

Materials

Yeast host recombinant human insulin, recombinant protein GAD 2, anti‐GAD65 (mouse anti‐human), and recombinant IA‐2 proteins were procured from Sigma‐Aldrich. Mouse anti‐human anti‐insulin, anti‐IA2 antibodies (mouse anti‐human), and goat anti‐mouse

FITC labeled IgG were procured from Millipore. PEGDA (Mn ≈ 6000), PEG (Mn ≈ 20,000), photoinitiator (2 - hydroxy - 4′ - (2 - hydroxyethoxy) - 2 methylpropiophenone), PBS, and BSA were procured from Sigma - Aldrich. Acrylate poly (ethylene) glycol succinimidyl carboxymethyl, Mn 5000, (ACRL - PEG - SCM - 5000) was obtained from Laysan Bio Inc. (Arab, AL).

Methods

To immobilize the antigens within the microgel, the antigens were incubated with 1.25 mg of ACRL - PEG - SCM - 5000 in PBS at room temperature for 3 h prior to use and discarded afterward. The prepolymer solution consisting of 100 μL of 8% (w/v) of PEG6000DA, 2% (w/v) photoinitiator, 10% (w/v) PEG 20K, and acrylated antigen was then loaded in the microfluidics for droplet generation.

The prepolymer solution was introduced at 1 μL min−1, and mineral oil was introduced at 15 μL min−1 to generate the droplets at the microfluidic cross - junction. When one of the generated droplets was flown in to the serpentine pockets, its trapping blocked the cross - serpentine flow and redirected the next droplet toward the following pocket sequentially. After trapping, droplets were exposed to ultraviolet light for crosslinking for 5 min (UVP CL - 1000 UV Oven, 365 nm). Then, BSA buffer was flown in at 30 μL min−1 to continuously wash the droplet for 30 min to prevent polydimethylsiloxane (PDMS) protein absorption. Lastly, PBS was flown in at 30 μL min−1 to continuously wash the droplets for 4 h to remove the unreacted

reagents and PEG porogens, thus creating the porous microgel.

For multiplexed detection, different prepolymers containing different acrylated antigens were loaded in the microfluidic tubing (Tygon tubing 1/16 in. ID) separated by mineral oil plugs. The prepolymers were then delivered into the microfluidics using a syringe pump to generate droplets. After generating and trapping droplets with the first prepolymer reagent, subsequent unwanted droplets were redirected to the waste channel. Then, the waste channel was closed to allow droplets with the second prepolymer containing the next acrylated antigen to be flown in and trapped in the next serpentine trap. The process continued until all three prepolymers containing the three different capture antigens were trapped in designated spots. These smart microgel droplets were then UV‐cured and washed as described above.

To run the multiplexed assays, smart microgels were incubated with appropriate antibodies at 20 μL min−1 flow rate for 60 min. Then, they were washed with TBST at 30 μL min−1 for 15 min and subsequently incubated with the reporter antibody at 30 μL min−1 for 40 min. Following this, droplets were washed again with TBST for 5 min and then imaged under the fluorescence microscopy.

After all the reactions between antigens, antibodies, and reporter antibody were completed, the smart microgel droplets were imaged under fluorescence microscopy for readout. The ratio of maximum center droplet intensity over background intensity was calculated using ImageJ to provide a normalized intensity value. The noise of the data is then the standard deviations of the normalized values. All optimization and cross‐reactivity were done in triplicates, while

the detection curve was done with five repeated runs. To generate the statistics, detections were compared to background by individual - samples t - test. The p - values (double sided) were provided for interpretation (Table S1, Supporting Information).

RESULTS AND DISCUSSION

Smart microgel optimizations were leveraged for the detection of diabetes antibodies by immobilizing capture antigens instead of capture antibodies. Detection chemistry, including diacrylated antigens in polyethylene diacrylate hydrogels and PEG porogen, was loaded into a microfluidic cross - junction **(Figure 7B)**. Flow from this aqueous phase was then pinched by mineral oil at the junction, creating an instability that ejects 500 μm droplets at a predictable frequency.50 Droplets then flowed down the serpentine channels and occupied individual trap sites one after another. However, in order to generate multiplexed detections for insulin, GAD, and IA - 2 antibodies in a single channel, droplets with different capture molecules were generated and sequentially trapped. This was achieved by directing the unwanted droplets toward a waste channel, then switching the flow toward the serpentine traps once desired droplets were generated **(Figure 7B)**. Upon trapping, the droplets were UV cured to immobilize the capture antigens and solidify the hydrogel for washing in PBS to remove porogens **(Figure 7C)**. With porosity - enhanced mass transport, unreacted porogen was thoroughly removed after 4.5 h of microfluidic perfusion, compared to the 24 h of incubation needed for bulk

preparations.[50] The resultant array **(Figure 7D)** represented a spatially multiplexed diabetes detection panel, without issues associated with spectral overlapping or computational imaging algorithms for shape‐coded techniques. After formation of the multiplexed smart microgels, the array was then ready to be assayed by flowing target antibodies, reporter antibodies, and washing steps, optimized in the following section.

Optimization of Reporter Incubation Time and Dilution Factor

The detections of all three antibodies shared a common reporter, FITC‐labeled IgG, whose incubation time and dilution factor were optimized using the insulin antibody detection. The fluorescence readout from the detection was quantified by the maximum droplet intensity divided by the background intensity, as illustrated by the line scan in **Figure 8A**. Using this quantification, reporter readout plateaued after 40 min of incubation **(Figure 8B)**. Furthermore, the reporter dilution showed lowered background and useful signal up to 1024 X dilution, which dramatically reduced the usage of reporter reagents **(Figure 8C)**. Based on these results, all subsequent experiments were carried out with 40 min of reporter incubation at 1024 X dilution. We anticipate the lower background from reporter dilution may help reduce nonspecific signals when moving to serum‐based detections in the future.

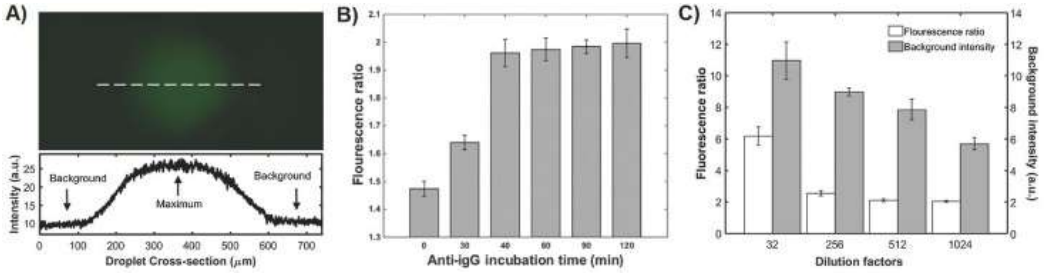

Figure 8. Reporter optimization. A) All fluorescence measurements were quantified by the ratio of maximum center intensity normalized by the background intensity, as seen by the line scan across a typical droplet. B) Fluorescence ratio of the reporter plateaued after 40 min of reporter incubation. C) While fluorescence ratio flattened after 256 times reporter dilution, the noise continued to drop. We selected the reporter dilution of 1024 times to reduce reagent consumption and minimize the background intensity, which would provide smaller standard deviations for more sensitive detections.

Optimization of Capture Antigens Concentration in PEGDA

After reporter optimization, the capture antigen concentration corresponding to each target antibody was optimized. All antigen optimizations were incubated with 1000 pg/mL target antibodies. **Figure 9A** illustrates the insulin capture antigen optimization, where the fluorescence ratio plateaued above a concentration of 200 pg/mL. GAD antigen optimization is shown in **Figure 9B**, where the fluorescence ratio showed a plateau above 500 pg/mL. Similarly, **Figure 9C** shows that IA‐2 concentration in poly(ethylene) glycol diacrylate (PEGDA) plateaus above 500 pg/mL. Optimization of antigen immobilization illustrated the differences of the binding epitopes between each antigen–antibody pair [23-36]. The subsequent experiments were run at their respective optimized antigen concentrations.

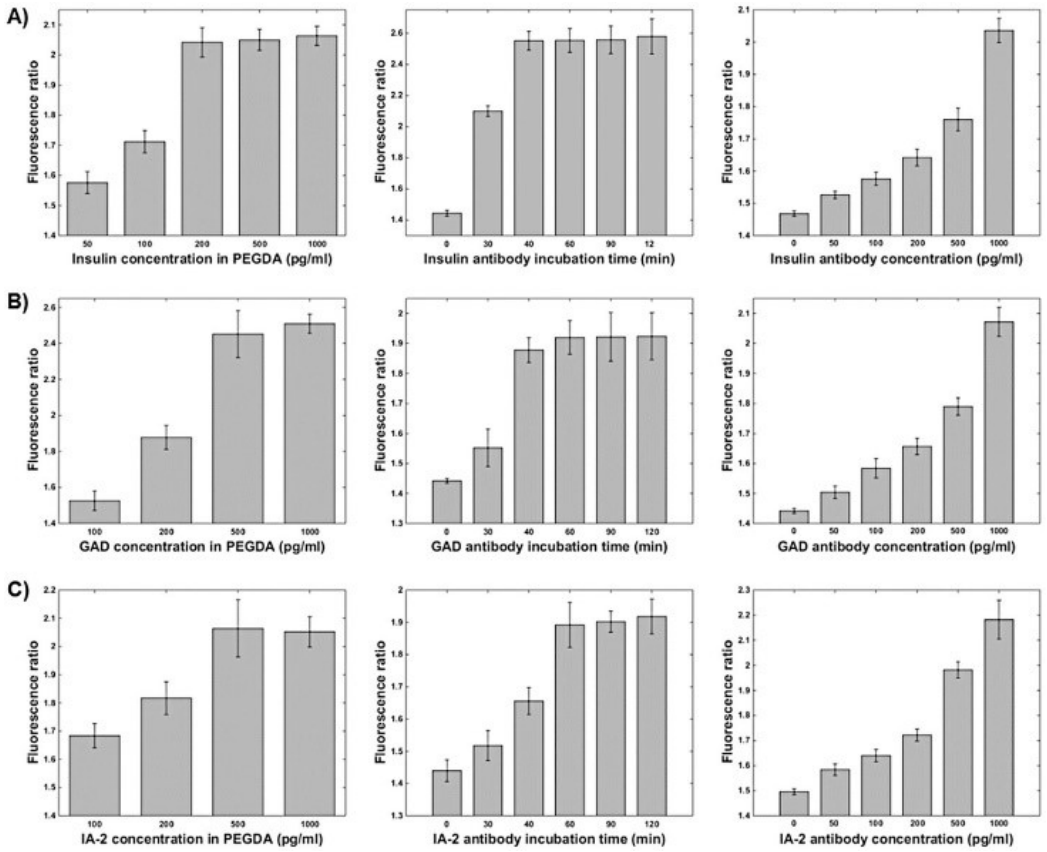

Figure 9. Diabetes panel optimization.

A) Insulin antibody detection was optimized with 200 pg/mL capture antigen immobilization, 40 min of analyte incubation, and a detectivity curve with a detection limit of 19.6 pg/mL. B) GAD antibody detection was optimized with a 500 pg/mL capture antigen immobilization, 40 min of analyte incubation, and a detectivity curve with a detection limit of 18.7 pg/mL. C) IA-2 antibody detection was optimized with a 500 pg/mL capture antigen immoblization, 60 min of analyte incubation, and a detectivity curve with a detection limit of 12.7 pg/mL. All capture antigen and analyte incubation optimizations were completed in triplicates. All detectivity curves were completed with five replicate runs. Error bars denote standard deviations.

Optimization of Target Antibodies Incubation Time

Next, we considered the kinetics of antibody–antigen binding within the smart microgels by optimizing the target antibody incubation times. Smart microgels immobilized with aforementioned antigen concentrations were incubated for various durations with their respective antibodies. The fluorescence ratio for insulin detection improved up to 40 min of target antibody incubation and plateaued thereafter **(Figure 9A)**. The same was seen for GAD antibody with a plateau after 40 min **(Figure 9B)**. IA‐2 and its antibody showed a different kinetics, as optimal incubation did not occur until after 60 min **(Figure 9C)**. We should also note that IA‐2 antibody is sensitive to buffer conditions, where glycine additives would increase nonspecific binding to the PEG hydrogel. Based on these optimizations, the longest incubation time was 60 min for the IA‐2 antibody, which we adopted for all subsequent singleplexed and multiplexed detections.

Characterizing the Limits of Antibody Detections

The assay protocol described above was optimized at 1000 pg/mL for respective diabetes antibodies. We subsequently tested the detectivity below this concentration to characterize the detection limits for each antibody. Concentrations of 50, 100, 200, 500, and 1000 pg/mL were assayed in five runs for each antibody, with error bars denoting standard deviations between each assay run at the particular concentration **(Figure 9)**. The detection limit was defined to be the concentration at which the signal rises three times the standard deviations of the zeroth

concentration. Using this definition, the insulin antibody detection limit was found to be 19.6 pg/mL **(Figure 9A)**. The GAD antibody detection limit was found to be 18.7 pg/mL **(Figure 9B)**. The IA‑2 antibody detection limit was found to be 12.7 pg/mL **(Figure 9C)**. Since the detection limit is a function of the background fluorescence and slope of the detectivity curve, minimization of reporter antibody contributed to these enhanced detection limits **(Figure 9C)**.

Characterization of Assay Specificity

To investigate whether other protein components in serum could potentially affect the fluorescence ratio, antigen immobilized microgel droplets were incubated with phosphate buffered saline (PBS), 0.1% bovine serum albumin (BSA), and their respective antibodies at 1000 pg/mL **(Figure 10)**. Antibody detections yielded fluorescence ratios higher than 2, whereas PBS and BSA yielded background levels of 1.5 or lower. More importantly, errors bars showed significant differences between specific and background detections with $p < 0.0001$. One reason for the low background without blocking is the bioinert nature of PEG hydrogel against nonspecific antibody binding. The result indicated that proteins other than targeted diabetes antibodies had minimum contributions toward the fluorescent signal, and also demonstrated that antigen functionalization without additional blocking is sufficient for smart microgel specificity.

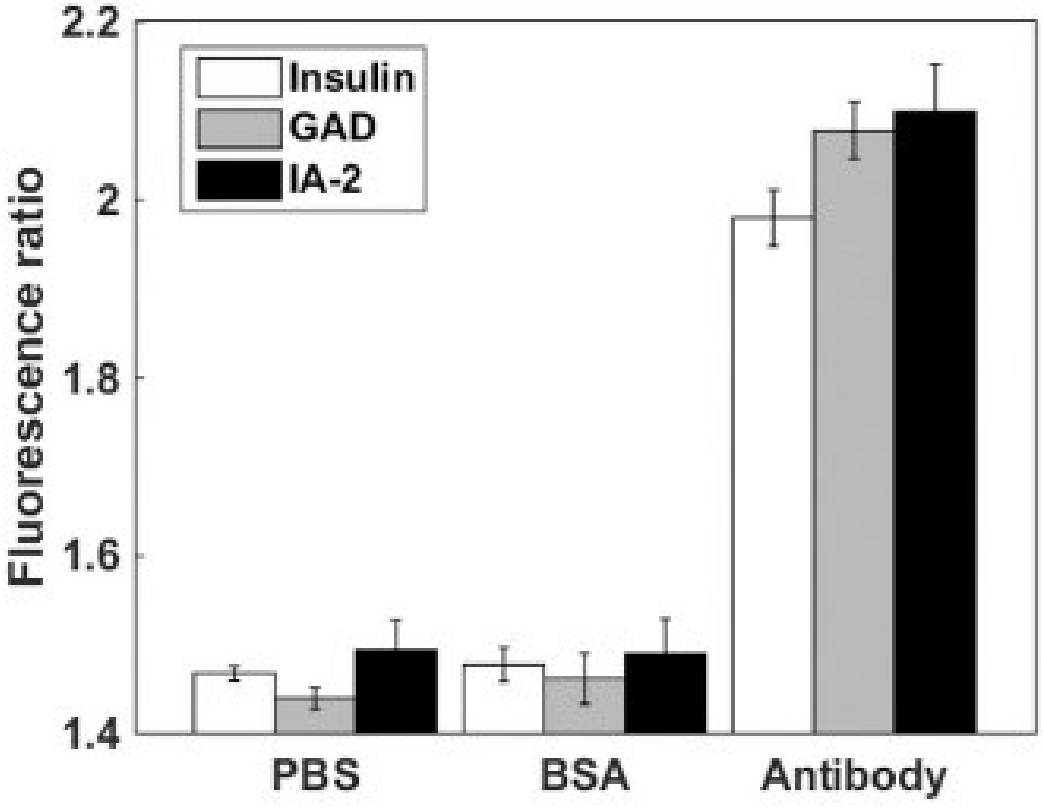

Figure 10. Antibodies assay specificity.

Nonspecific binding to BSA resulted in fluorescence ratios on par with PBS background. Specific antibody detections resulted in a ratio around 2 versus 1.5 of background. Moreover, significant differences between detections and background yielded a $p < 0.0001$.

Characterization of Singleplex and Duplex Cross‐Reactivity

One major difficulty in assaying multiple antibodies within one sample assay volume is the cross‐reactivity among the target antibodies and nontarget proteins. First, microgel droplets of all target antigens were incubated with each target antibody one at a time at 1000 pg/mL to evaluate antigen–antibody cross‐reactivity **(Figure 11)**. For reference, background

fluorescence ratios for each antigen (zero antibody concentrations) were typically below 1.5, as seen from their detectivity curves. In comparison, the on‐target antigen–antibody detections, e.g., insulin to insulin antibody, yielded a ratio close to 2, significantly higher than the background ($p < 0.0001$, complete comparisons in Table S1, Supporting Information). After analysis of singleplex cross‐reactivity, combinations of two antibodies each at 1000 pg/mL were assayed **(Figure 12)**. As singleplex cross‐reactivity showed negligible nonspecific bindings between antibody and capture antigens, this duplex assay tested the possibility of unintended antibody to antibody interactions. Again, the on‐target pairs yielded fluorescence ratios close to 2, while miss‐matched backgrounds remained below 1.5. For example, the GAD to insulin+GAD antibodies fluorescence ratio was significantly higher than that of the IA‐2 mismatched with insulin+GAD antibodies.

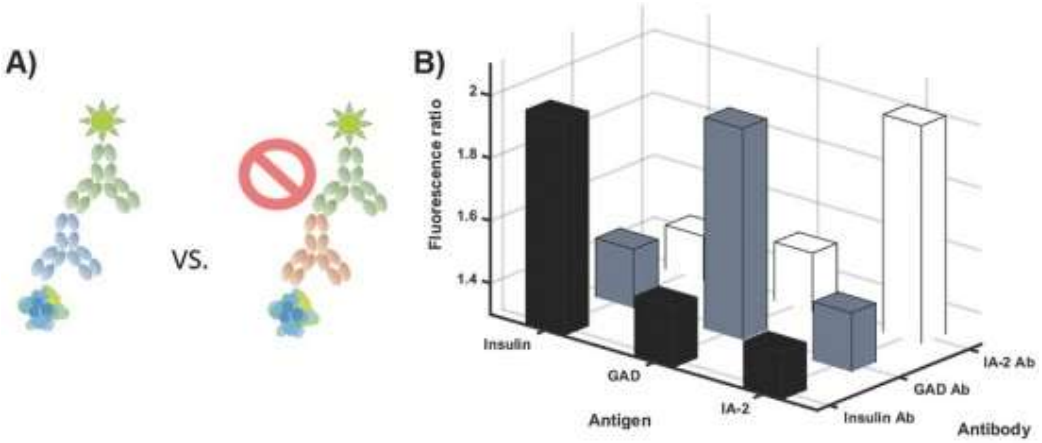

Figure 11. Singleplex cross-reactivity.

A) Cross-reactivity between target (blue) and nontarget (orange) antibodies are tested one at a

time to investigate nonspecific antibody–antigen interactions. B) This test showed that nonspecific antibody–antigen reactions yielded fluorescence ratios similar to that of background at ≈1.5.

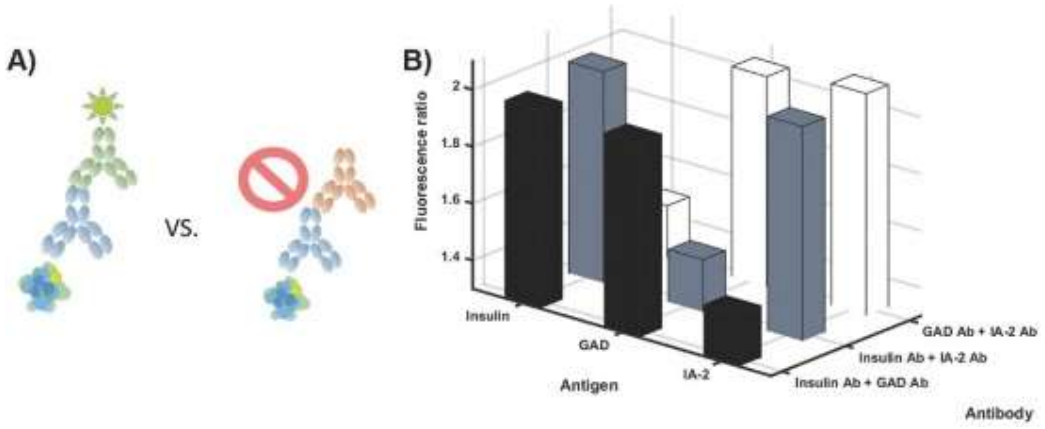

Figure 12. Duplex cross-reactivity.

A) Cross-reactivity between combinations of antibodies pairs tested nonspecific antibody–antibody interactions. B) This test showed that nonspecific antibody–antibody reactions did not affect the on-target antibody–antigen detections.

Muliplexed Detection and Quantitative Protein Recovery

After confirming negligible cross‐reactivities at elevated antibody concentrations, we demonstrated multiplexed detections of insulin, GAD, and IA‐2 antibody concentrations and their quantifications simultaneously. Three concentrations of 50, 200, and 500 pg/mL were assayed for each target antibody in multiplexed droplets. Triplicates were run for each condition. However, since the detections were multiplexed, the entire assay took a total of just

nine runs. The measured concentrations were within 15% of the designated values (Table 1).

Target concentration [pg/mL]			Retrieved concentration [pg/mL]		
Insulin Ab	GAD Ab	IA-2 Ab	Insulin Ab	GAD Ab	IA-2 Ab
50	50	50	48 ± 11.4	45 ± 7.1	51.8 ± 9.8
200	200	200	204 ± 22.8	201.4 ± 17.8	203.3 ± 26.3
500	500	500	494.9 ± 41.7	521.28 ± 26.24	520 ± 39.5

Table 1. Multiplexed protein detections with target concentrations of 50, 200, and 500 pg/mL for all three antibodies simultaneously

CONCLUSION

We have achieved a multiplexed detection panel for diabetes antibodies targeting insulin, GAD, and IA‐2. The assay can be prepared in 4.5 h prior to running the assay, with a total assay time of just 2 h for all three parameters in a single sample. For all target antibodies, a detection limit better than 20 pg/mL was achieved, representing the detection of only 8‐30 thousand molecules in each microgel droplet. Singleplex and multiplex detections showed negligible cross‐reactivity. Multiplexed detections were within 15% of the target concentrations. The serpentine microfluidic achieved a spatial multiplexing of the microgels that avoided issues associated with spectral or imaging based techniques. The resultant

detection panel has the potential to improve diabetes detection, as well as investigate immunogenic mechanisms in diabetes.

Chapter 4. Beta Cells Gradient Insulin Sensor

INTRODUCTION

This study is mainly focusing on microfluidic oxygen gradient with multimodal stimulations and detections to investigate a possible link between hypoxia and free fatty acid (FFA) exposures in beta cell impairments and apoptosis. Distinct from the autoimmune pathology in type I diabetes, type II diabetes development relating to beta cell dysfunction is not well understood due to the numerous pathological mechanisms and many risk factors. These risk factors often coexist in obesity and could possibly interact synergistically. For example, elevated FFA in obesity can lead to insulin deficiency, though only a fraction of people with high FFA develop diabetes. On the other hand, hypoxia can also suppress insulin secretion, but no clear mechanism leading to the development of diabetes has been discovered. Intriguingly, recent studies suggest that both FFA and hypoxia exacerbate beta cell ER stress via the unfolded protein response (UPR) pathways, possible through reactive oxygen species (ROS). However, neither factor was sufficient to induce beta cell apoptosis alone . This suggests that a synergistic effect might exist, as hypoxia also affects FFA levels in vivo . Despite suggestive evidences of this FFA-hypoxia link, however, its potential role in islet pathophysiology has not been

demonstrated. One reason is the lack of proper techniques for controlling hypoxia at the microscale level of beta cells. Standard hypoxic chambers cannot generate a gradient to test multiple exposures, nor can they provide in situ microscopy of beta functions. PI's previous work has demonstrated novel microfluidic devices to provide simultaneous hypoxia and glucose stimulations with real-time microscopy monitoring. Proposed here is a new device with integrated oxygen gradient for hypoxia and FFA exposures. It incorporates an open-top design to allow easy access for normal cell culturing and assay reagent exchange. Furthermore, a novel hydrogel sensor film is layered directly beneath the cells to provide in situ spatial insulin detections, in addition to spatial monitoring of Ca2+ and ROS via microscopy **(Figure 13)**. The spatial insulin detection can be correlated to the hypoxia gradient directly, a challenging feat to achieve in situ. By proving the hypothesis of FFA-hypoxia synergy in inducing beta cell impairment and apoptosis, a potential mechanism can be proposed towards the complicated development of type II diabetes.

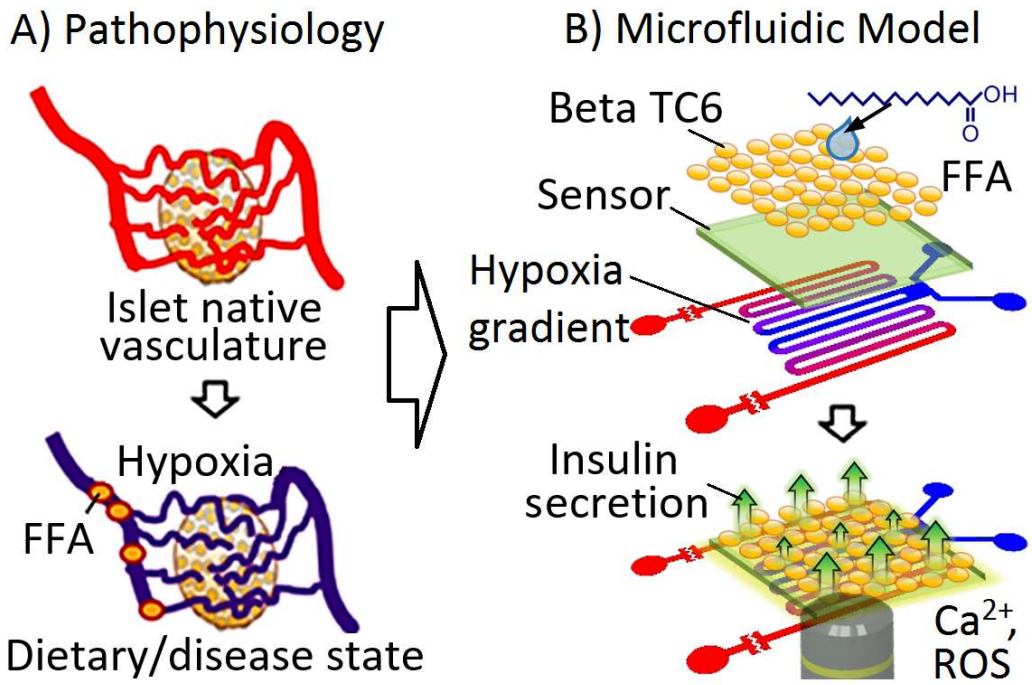

Figure 13. Testing hypoxia-FFA synergy via culturing beta cells in multimodal microfluidics.

A) Pancreatic islet beta cells are well-vascularized. When cells are exposed to hypoxia and FFA, insulin secretion and cell survival may be impaired. B) To study hypoxia-FFA interaction, a stimulation sandwich is created around beta cells with built-in insulin sensor to compliment Ca^{2+} and ROS microscopy.

MATERIALS AND METHODS

Meterails

Poly (ethylene glycol) diacrylate (PEGDA) (Min.~6000, referred as PEG6000DA), poly (ethylene glycol) (PEG) (Min.~20,000), 2-Hydroxy-4′-(2-hydroxyethoxy)-2-

methylpropiophenone, insulin, mineral oil, phosphate buffer saline (PBS), and IgG from human serum were procured from Sigma-Aldrich (St. Louis, MO). Anti-insulin was procured from Millipore. Polydimethylsiloxane (PDMS) was obtained from Ellsworth adhesives and SU8 2100 was purchased from MicroChem.

Methods

The microfluidic based gas gradient devices was fabricated using the method mentioned in chapter 1, and then bond a boundary PDMS rectangular cover on the top of gas gradient diffusion layer channel part, in this way created a chamber that include the channel part to enhance the PEGDA pre-polymer solution loaded and cured.

To immobilize the antigens within the PEGDA hydrogel layer, the anti-insulin were incubated with 1.25 mg of ACRL-PEG-SCM-5000 in PBS at room temperature for 3 h prior to use and discarded afterward. The prepolymer solution consisting of 100 μL of 8% (w/v) of PEG6000DA, 2% (w/v) photoinitiator, 10% (w/v) PEG 20K, and acrylated antigen was then loaded in the microfluidics for droplet generation.

The pre-polymer solution loaded on the gas gradient diffusion layer, then cover the pre-polymer solution with a piece of PDMS slice. The PEGDA pre-polymer solution were exposed to ultraviolet light for crosslinking for 5 min (UVP CL-1000 UV Oven, 365 nm). Then, the device chamber was incubated with BSA for 1 hour to prevent polydimethylsiloxane (PDMS) protein absorption. Lastly, use PBS to continually washing the hydrogel layer for 4 h to remove

the unreacted reagents and PEG porogens, thus creating the porous microgel. Then incubate the hydrogel with various concentration of insulin for 20 to 120 minutes, washed the hydrogel with TBST buffer for 3 times, each time for 10 minutes. After that, incubated the hydrogel with various insulin reporter concentration for 20 to 120 minutes, washed with TBST buffer for 3 times, each time for 5 minutes. Then take image under fluorescence microscopy.

RESULTS AND DISCUSSION

Optimization of anti-insulin concentration in PEGDA

PEGDA hydrogel layer immobilized with various anti-insulin concentrations were incubated with 1000 pg/mL insulin. The fluorescence ratio for anti-insulin detection improved up to 200pg/mL of insulin incubation and plateaued thereafter **(Figure 14A)**. Based on the optimization, the lowest concentration of anti-insulin in PEGDA hydrogel is 200 pg/mL, which we adopted for all subsequent experiments.

Optimization of insulin and insulin reporter incubation time

Then we optimized the incubation time of insulin and insulin reporter antibody. The fluorescence ratio plateaued after 30 minutes incubation of insulin and 60 minutes incubation of insulin reporter **(Figure 14B, 14C)**. Based on the result of incubation time, the shortest assay period would be less than 2 hours.

Characterizing the Limits of insulin Detections

We tested the detectivity of insulin below 1000 pg/mL to characterize the detection limits for each antibody. Concentrations of 50, 100, 200, 500, and 1000 pg/mL were assayed in five runs for each antibody, with error bars denoting standard deviations between each assay run at the particular concentration. The detection limit was defined to be the concentration at which the signal rises three times the standard deviations of the zeroth concentration. Using this definition, the insulin detection limit was found to be lower than 50 pg/mL **(Figure 14D)**.

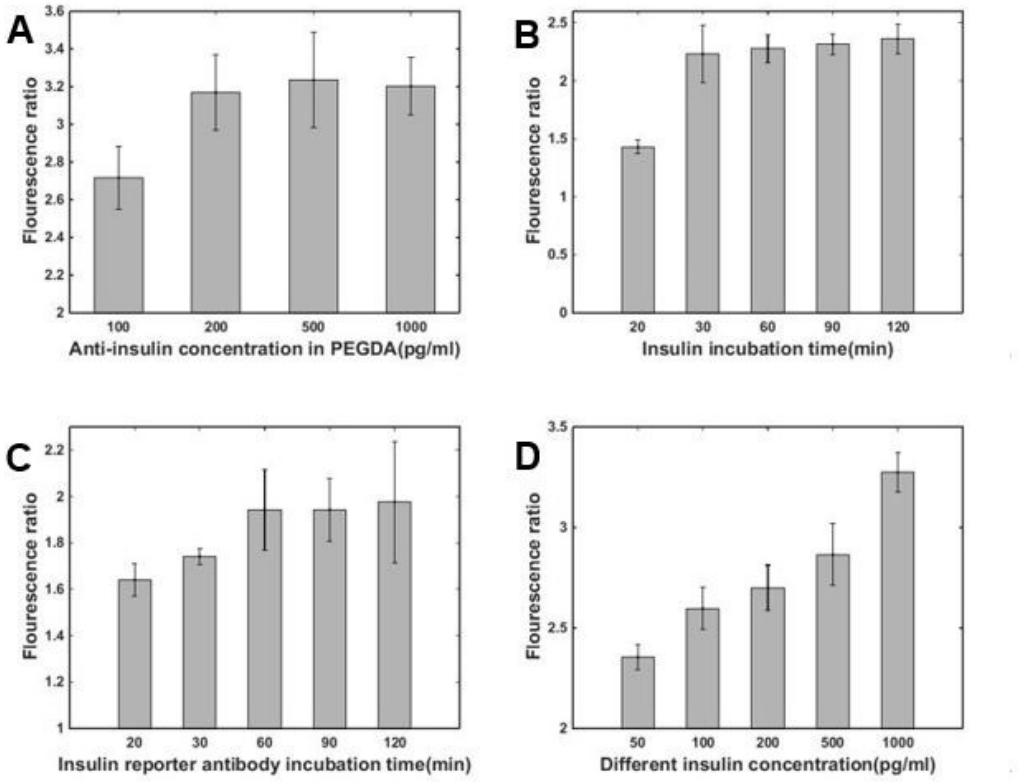

Figure 14. Optimization of insulin secretion sensor.

(A) The lowest insulin antibody concentration in PEGDA was optimized to be 200 pg/mL with 1000 pg/mL insulin incubation (B) insulin protein incubation times above 30 min reaches a stable signal readout. (C) Reporter incubation times above 60 min reaches a stable signal readout. Thus, 30 min insulin and 60 min reporter incubation times were used to for subsequents insulin detections. (D) Insulin detection yielded a detection curve from 50 to 1000 pg/mL. Using this trend, a detection limit better than 50 pg/mL was abtained.

CONCLUSION

The insulin sensor was well optimized in this assay, we have achieved a fasten and sensitive detection for beta cells insulin secretion, it's a big progress for our next step, to culture the cells on hydrogel, apply hypoxia and FFA stimulation. For the detection of insulin, better than 50 pg/ml detection limit was achieved, the assay can be finished within 2 hours which is good for beta cells. It confirmed that our insulin detection sensor will be well applied in this project for researching the hypoxia and FFA stimulation of beta cells.

Chapter 5. Conclusion

In this thesis, three projects was designed and finished mainly focusing on the diabetes. First, we leveraged a microfluidic scaling with enhanced molecule transport of porous microgel within an integrated serpentine trapper array, a rapid and sensitive detection of VEGF measurement is achieved, with a 0.9 pg/ml detection limit and only 1+ hour of assay time. In human wound healing especially in wound healing of diabetic uclers, VEGF play an important role as a biomarkers, our technic provide a fast and sensitive measurement in biomedical diagnostics. Then using our microfluidic microgel panel, a multiple detection for antibodies targeting insulin, GAD, IA-2 was achieved, and for all target antibodies, a detection limit better than 20 pg/ml was achieved with a total time of 2 hours for all three parameters in a single sample, provide a multiple detection of diabetes autoantibodies in type 1 diabetes diagnostics. In the last part, a insulin sensor based on gas gradient microfluidic was leveraged, can detect the insulin secretion from beta cell with better than 50 pg/ml detection limit and 2 hours assay time, enable a fast detection for beta cells under hypoxia and FFA stimulation.

By taking the advances of microfluidic and porous PEGDA hydrogel, we are making major progress in diabetes related diseases diagnostics and monitoring, towards better understanding of its complex mechanisms and potential therapeutic strategies.

REFERENCES

1. C. Törn, P. W. Mueller, M. Schlosser, E. Bonifacio, P. J. Bingley, Diabetologia 2008, 51, 846.
2. T. P. Staeva, L. Chatenoud, R. Insel, M. A. Atkinson, Diabetes 2013, 62, 9.
3. J. M. Wenzlau, J. C. Hutton, Curr. Diabetes Rep. 2013, 13, 608.
4. C. J. Greenbaum, J. P. Palmer, B. Kuglin, H. Kolb, J. Clin. Endocrinol. Metab. 1992, 74, 1040.
5. M. Schlosser, P. W. Mueller, C. Törn, E. Bonifacio, P. J. Bingley, Diabetologia 2010, 53, 2611.
6. V. Lampasona, M. Schlosser, P. W. Mueller, A. J. Williams, J. M. Wenzlau, J. C. Hutton, P. Achenbach, Clin. Chem. 2011, 57, 1693.
7. P. J. Bingley, E. Bonifacio, P. W. Mueller, Diabetes 2003, 52, 1128.
8. M. A. Atkinson, N. K. Maclaren, W. J. Riley, W. E. Winter, D. D. Fisk, R. P. Spillar, Diabetes 1986, 35, 894.
9. A. J. Williams, V. Lampasona, M. Schlosser, P. W. Mueller, D. L. Pittman, W. E. Winter, B. Akolkar, R. Wyatt, C. Brigatti, S. Krause, P. Achenbach, Diabetes 2015, 64, 3239.
10. C. Andersson, M. Kolmodin, S. A. Ivarsson, A. Carlsson, G. Forsander, B. Lindblad, J. Ludvigsson, I. Kockum, C. Marcus, U. Samuelsson, E. Örtqvist, Pediatr. Diabetes 2014, 15, 336.
11. J. M. LaGasse, M. S. Brantley, N. J. Leech, R. E. Rowe, S. Monks, J. P. Palmer, G. T. Nepom, D. K. McCulloch, W. A. Hagopian, Diabetes Care 2002, 25, 505.
12. C. F. Verge, R. Gianani, E. Kawasaki, L. Yu, M. Pietropaolo, H. P. Chase, G. S. Eisenbarth, R. A. Jackson, Diabetes 1996, 45, 926.
13. A. G. Ziegler, S. Schmid, D. Huber, M. Hummel, E. Bonifacio, JAMA 2003, 290, 1721.
14. Z. Zhao, D. Miao, A. Michels, A. Steck, F. Dong, M. Rewers, L. Yu, J. Immunol. Methods 2016, 430, 28.
15. B. Zhang, R. B. Kumar, H. Dai, B. J. Feldman, Nat. Med. 2014, 20, 948.
16. L. Herszenyi, Z. Tulassay, Dig. Dis. 2012, 30, 201.
17. L. Yu, D. T. Robles, N. Abiru, P. Kaur, M. Rewers, K. Kelemen, G. S. Eisenbarth, Proc. Natl. Acad. Sci. USA 2000, 97, 1701.
18. P. J. Bingley, E. Bonifacio, A. G. Ziegler, D. A. Schatz, M. A. Atkinson, G. S. Eisenbarth, Diabetes Care 2001, 24, 398.
19. A. D. Liese, R. B. D'Agostino Jr, R. F. Hamman, P. D. Kilgo, J. M. Lawrence, L. L. Liu,

B. Loots, B. Linder, S. Marcovina, B. Rodriguez, D. Standford, D. E. Williams, 2006, 118, 1510.
20. C. C. Patterson, G. G. Dahlquist, E. Gyürüs, A. Green, G. Soltész, Lancet 2009, 373, 2027.
21. K. G. M. M. Alberti, P. Z. Zimmet, Diabetic Med. 1998, 15, 539.
22. E. Bonifacio, Diabetes Care 2015, 38, 989.
23. M. J. Kracht, A. Zaldumbide, B. O. Roep, Trends Endocrinol. Metab. 2016, 27, 353.
24. S. M. Trigwell, P. M. Radford, S. R. Page, A. C. Loweth, R. F. James, N. G. Morgan, I. Todd, Clin. Exp. Immunol. 2001, 126, 242.
25. M. van Lummel, G. Duinkerken, P. A. van Veelen, A. de Ru, R. Cordfunke, A. Zaldumbide, I. Gomez-Touriño, S. Arif, M. Peakman, J. W. Drijfhout, B. O. Roep, Diabetes 2014, 63, 237.
26. J. W. McGinty, I. T. Chow, C. Greenbaum, J. Odegard, W. W. Kwok, E. A. James, Diabetes 2014, 63, 3033.
27. I. Kharroubi, L. Ladrière, A. K. Cardozo, Z. Dogusan, M. Cnop, D. L. Eizirik, Endocrinology 2004, 145, 5087.
28. D. R. Laybutt, A. M. Preston, M. C. Åkerfeldt, J. G. Kench, A. K. Busch, A. V. Biankin, T. J. Biden, Diabetologia 2007, 50, 752.
29. S. C. Martinez, K. Tanabe, C. Cras-Méneur, N. A. Abumrad, E. Bernal-Mizrachi, M. A. Permutt, Diabetes 2008, 57, 846–59.
30. K. Maedler, G. A. Spinas, D. Dyntar, W. Moritz, N. Kaiser, M. Y. Donath, Diabetes 2001, 50, 69.
31. D. A. Cunha, P. Hekerman, L. Ladrière, A. Bazarra-Castro, F. Ortis, M. C. Wakeham, F. Moore, J. Rasschaert, A. K. Cardozo, E. Bellomo, L. Overbergh, J. Cell Sci. 2008, 121, 2308.
32. B. O. Roep, M. J. Kracht, M. van Lummel, A. Zaldumbide, Curr. Opin. Immunol. 2016, 43, 67.
33. M. S. Horwitz, L. M. Bradley, J. Harbertson, T. Krahl, J. Lee, N. Sarvennick, Nat. Med. 1998, 4, 781.
34. B. T. Kurien, R. H. Scofield, Autoimmun. Rev. 2008, 7, 567.
35. D. L. Kaufman, M. Clare-Salzler, J. Tian, T. Forsthuber, G. S. Ting, P. Robinson, M. A. Atkinson, E. E. Sercarz, A. J. Tobin, P. V. Lehmann, Nature 1993, 366, 69.
36. S. Hong, M. T. Wilson, I. Serizawa, L. Wu, N. Singh, O. V. Naidenko, T. Miura, T. Haba, D. C. Scherer, J. Wei, M. Kronenberg, Nat. Med. 2001, 7, 1052.
37. L. Yu, D. Miao, L. Scrimgeour, K. Johnson, M. Rewers, G. S. Eisenbarth, Diabetes 2012, 61, 179.
38. R. Hilbrands, V. A. Huurman, P. Gillard, J. H. L. Velthuis, M. De Waele, C. Mathieu, L. Kaufman, M. Pipeleers-Marichal, Z. Ling, B. Movahedi, D. Jacobs-Tulleneers-Thevissen, D. Monbaliu, D. Ysebaert, F. K. Gorus, B. O. Roep, D. G. Pipeleers, B. Keymeulen, Diabetes 2009, 58, 2267.
39. Mayo Medical Laboratories, Mayo Medical Laboratories Interpretive Handbook, Mayo Medical Laboratories, Rochester, NY, USA 2005.

40. D. Miao, K. M. Guyer, F. Dong, L. Jiang, A. K. Steck, M. Rewers, G. S. Eisenbarth, L. Yu, Diabetes 2013, 62, 4174.
41. L. Yu, F. Dong, D. Miao, A. R. Fouts, J. M. Wenzlau, A. K. Steck, Diabetes Care 2013, 36, 2266.
42. M. Evans, C. Sewter, E. Hill, Assay Drug Dev. Technol. 2003, 1, 199.
43. J. P. Nolan, L. A. Sklar, Trends Biotechol. 2002, 20, 9.
44. S. C. Chapin, D. C. Pregibon, P. S. Doyle, Lab Chip 2009, 9, 3100.
45. L. Wang, C. Yang, W. Tan, Nano Lett. 2005, 5, 37.
46. B. He, S. J. Son, Anal. Chem. 2007, 79, 5257.
47. S. Birtwell, Integr. Biol. 2009, 1, 345.
48. A. Al-Ameen, G. Ghosh, Biosens. Bioelectron. 2013, 49, 105.
49. M. A. Al-Ameen, J. Li, D. G. Beer, G. Ghosh, Analyst 2015, 140, 4530.
50. Z. Zhao, M. A. Al-Ameen, K. Duan, G. Ghosh, J. F. Lo, Biosens. Bioelectron. 2015, 74, 305.
51. K. Duan, G. Ghosh, J. F. Lo, in MicroTAS (Eds. N. Pamme, J. Ducree) The Chemical and Biological Microsystems Society, Washington, DC, USA 2016 p. 956.
52. G. Huang, Y. Xiang, L. Pan, X. Li, S. Luo, Z. Zhou, Diabetes/Metab. Res. Rev. 2013, 29, 363.
53. F. K. Gorus, E. V. Balti, I. Vermeulen, S. Demeester, A. Van Dalem, O. Costa, H. Dorchy, S. Tenoutasse, T. Mouraux, C. De Block, P. Gillard, Clin. Exp. Immunol. 2013, 171, 82.
54. M. Fabris, S. Zago, M. Liguori, M. T. Trevisan, M. Zanatta, A. Comici, G. Zanette, E. Carlin, F. Curcio, E. Tonutti, Autoimmun. Highlights 2015, 6, 17.
55. J. Kopecˇek, Biomaterials 2007, 28, 5185.
56. E. Cosgriff-Hernandez, M. S. Hahn, B. Russell, T. Wilems, D. Munoz-Pinto, M. B. Browning, J. Rivera, M. Höök, Acta Biomater. 2010, 6, 3969.
57. M. C. Branco, D. J. Pochan, N. J. Wagner, J. P. Schneider, Biomaterials 2010, 31, 9527.
58. S. Frokjaer, D. E. Otzen, Nat. Rev. Drug Discovery 2005, 4, 298.
59. M. Ye, S. Kim, K. Park, J. Controlled Release 2010, 146, 241.
60. R. E. Sallach, W. Cui, F. Balderrama, A. W. Martinez, J. Wen, C. A. Haller, J. V. Taylor, E. R. Wright, R. C. Long, E. L. Chaikof, Biomaterials 2010, 31, 779.
61. L. Li, Q. Wang, J. Feng, L. Tong, B. Tang, Anal. Chem. 2014, 86, 5101.
62. H. Zhang, G. Jenkins, Y. Zou, Z. Zhu, C. J. Yang, Anal. Chem. 2012, 84, 3599.
63. E. Brouzes, M. Medkova, N. Savenelli, D. Marran, M. Twardowski, J. B. Hutchison, J. M. Rothberg, D. R. Link, N. Perrimon, M. L. Samuels, Proc. Natl. Acad. Sci. 2009, 106, 14195.
64. Huebner, M. Srisa-Art, D. Holt, C. Abell, F. Hollfelder, J. B. Edel, Chem. Commun. 2007, 12, 1218.
65. D. Chen, W. Du, Y. Liu, W. Liu, A. Kuznetsov, F. E. Mendez, L. H. Philipson, R. F. Ismagilov, Proc. Natl. Acad. Sci. 2008, 105, 16843.
66. C. J. Easley, J. V. Rocheleau, W. S. Head, D. W. Piston, Anal. Chem. 2009, 81, 9086.

67. Al-Ameen, M.A., Ghosh, G., 2013. Biosens. Bioelectron. 49, 105–110.
68. Bao, P., Kodra, A., Tomic-Canic, M., Golinko, M.S., Ehrlich, H.P., Brem, H., 2009. J.
69. Surg. Res. 153 (2), 347–358.
70. Birtwell, S., Morgan, H., 2009. Integr. Biol. 1, 345.
71. Brouzes, E., Medkova, M., Savenelli, N., Marran, D., Twardowski, M., Hutchison, J.B., Rothberg, J.M., Link, D.R., Perrimon, N., Samuels, M.L., 2009. Proc. Natl. Acad. Sci. 106 (34), 14195–14200.
72. Byrne, A.M., Bouchier-Hayes, D.J., Harmey, J.H., 2005. J. Cell. Mol. Med. 9, 777–794.
73. Chapin, S.C., Pregibon, D.C., Doyle, P.S., 2009. Lab Chip 9, 3100–3109.
74. Chen, D., Du, W., Liu, Y., Liu, W., Kuznetsov, A., Mendez, F.E., Philipson, L.H., Ismagilov, R.G., 2008. Proc. Natl. Acad. Sci 105 (44), 16843–16848.
75. Chen, H., Hou, Y., Qi, F., Zhang, J., Koh, K., Shen, Z., Li, G., 2014. Biosens. Bioelectron. 61, 83–87.
76. Crawshaw, A.A., Griffiths, C.E.M., Young, H.S., 2012. Exp. Opin. Investig. Drugs 21, 33–43.
77. Dishinger, J.F., Reid, K.R., Kennedy, R.T., 2009. Anal. Chem. 81 (8), 3119–3127.
78. Eisenstein, M., 2006. Nature 444, 959–962.
79. Evans, M., Sewter, C., Hill, E., 2003. Assay Drug Dev. Technol. 1, 199–207.
80. Farrera, N., 2004. Endocr. Rev. 25, 581–611.
81. Gao, W., Kuick, R., Orchekowski, R.P., Misek, D.E., Qiu, J., Greenberg, A.K., Rom, W.N., Brenner, D.E., Omenn, G.S.S., Haab, B.B., Hanash, S.M., 2005. BMC Cancer 5, 110.
82. Garstecki, P., Gitlin, I., Diluzio, W., Whitesides, G., Kumacheva, E., Stone, H., 2004.
83. Appl. Phys. Lett. 85, 2649–2651.
84. Ghosh, G., Lee, A.G., Palecek, S.P., 2009. Anal. Biochem. 393, 205–214.
85. Ghosh, G., Yan, X., Lee, A.G., Korn, S.J., Palecek, S.P., 2010. Biosens. Bioelectron. 26, 424–431.
86. He, B., Son, S.J., Lee, S.B., 2007. Anal. Chem. 79, 5257–5263.
87. Hoeben, A., Landuyt, B., Highley, M.S., Wildiers, H., Van Oosterom, A.T., De Bruijn, E. A., 2004. Pharmacol. Rev. 56, 549–580.
88. Huebner, A., Srisa-Art, M., Holt, D., Abell, C., Hollfelder, F., deMelloc, A.J., Edel, J.B., 2007. Chem. Comm., 1218–1220.
89. Khademhosseini, A., Langer, R., 2007. Biomaterials 28 (34), 5087–5092.
90. Lee, S.S., Joo, Y.S., Kim, W.U., Min, D.J., Min, J.K., Park, S.H., Cho, C.S., Kim, H.Y., 2001. Clinical and Experimental Rheumatology 19, 321–324.
91. Lee, H.J., Wark, A.W., Corn, R.M., 2008. Analyst 133, 975–983.
92. Lin, C.W., Wei, K.C., Liao, S.S., Huang, C.Y., Sun, C.,L., Wu, P.J., Lu, Y.J., Yang, H.W., Ma, C.C., 2015. Biosens. Bioelectron. 67, 431–437.
93. Mattoon, D., Michaud, G., Merkel, J., Schweitzer, B., 2005. Exp. Rev. Prot. 2, 879–889.
94. Mazutis, L., Baret, J.-C., Treacy, P., Skhiri, Y., Araghi, A.F., Ryckelynck, M., Taly, V., Griffiths, A.D., 2009. Lab Chip 9, 2902–2908.
95. Nemir, S., Hayenga, H.N., West, J.L., 2010. Biotechnol. Bioeng. 105, 636–644.

96. Nolan, J.P., Sklar, L.A., 2002. Trends Biotechnol. 20, 9–12.
97. Nourmohammadzadeh, M., Lo, J.F., Bochenek, M., Mendoza-Elias, J.E., Wang, Q., Li, Z., Zheng, L., Qi, M., Eddington, D.T., Oberholzer, J., Wang, Y., 2013. Anal. Chem. 85 (23), 11240–11249.
98. Pasquardini, L., Pancheri, L., Potrich, C., Ferri, A., Piemonte, C., Lunelli, L., Napione, L., Comunanza, V., Alvaro, M., Vanzetti, L., Bussolino, F., Pederzolli, C., 2015. Biosens. Bioelectron. 68, 500–507.
99. Prabhulkar, S., Alwarappan, S., Liu, G., Li, C.-Z., 2009. Biosens. Bioelectron. 24, 3524–3530.
100. Rapisarda, A., Melilo, G., 2012. Adv. Cancer Res. 114, 237–267.
101. Rozman, A., Silar, M., Kosnik, M., 2012. Radiol. Oncol. 46, 354–359.
102. Tang, W.H., Takeuchi, S., 2007. Adv. Mater. 19, 2696–2701.
103. Wang, S.E., Huang, Y., Hu, K., Tian, J., Zhao, S., 2014. Anal. Method. 6, 62–66.
104. Wang, S.E., Si, S., 2013. Appl. Spectrosc. 67 (11), 1270–1274.
105. Wang, T., Lacik, I., Brissova, M., Anilkumar, A.V., Prokop, A., Hunkeler, D., Green, R., Shahrokhi, K., Powers, A.C., 1997. Nat. Biotechnol. 15 (4), 358–362.
106. Wang, L., Yang, C., Tan, W., 2005. Nano Lett. 5, 37–43.